

STRUCTURAL PROPERTIES OF GIANT H II REGIONS IN NEARBY GALAXIES

ROBERT C. KENNICUTT, JR.¹

Department of Astronomy, University of Minnesota

Received 1984 April 20; accepted 1984 June 19

ABSTRACT

Balmer emission-line and radio continuum maps of nearby giant extragalactic and Galactic H II regions have been used to define their basic physical properties. Even within the relatively narrow range of galaxy types studied here, the luminosities, masses, and densities of the largest H II regions range over several orders of magnitude. Hence the term “giant H II region” encompasses a physically diverse collection of objects. By combining maps of the extragalactic H II regions with radio continuum maps of the largest Galactic objects, it has been possible to compare these objects on comparable spatial resolutions. While analogs to the largest known Galactic objects have been found in nearby galaxies, the apparent absence of very bright 30 Doradus-type H II regions in the Galaxy is almost certainly a real effect. While there is some statistical evidence that suggests that there may exist a distinct class of “supergiant” H II regions, the physical properties of the largest H II regions merge smoothly with those of the less luminous giant H II regions, including the largest Galactic objects. Despite the large variation in the structure and integrated properties of the largest H II regions in different galaxies, the properties of objects in any individual galaxy are relatively homogeneous, suggesting that the galactic environment is an important parameter influencing the structure and evolution of the H II regions.

Subject headings: galaxies: structure — nebulae: H II regions — radio sources: galaxies

I. INTRODUCTION

Giant H II regions have been applied extensively as tracers of chemical composition, star formation, and spiral structure in galaxies, and as extragalactic distance indicators, but in spite of this broad application relatively little is known about the physical properties of the H II regions themselves. The current controversy regarding the ionization sources of the largest objects has led to a renewed interest in the giant H II regions, and to a need for hard data on their basic physical properties. Excellent data for a few objects are available from radio continuum surveys (e.g., Israel 1976), but the limited sensitivity and resolution of these surveys limit the kinds of H II regions that can be studied.

In this paper I have used H α emission-line maps and published radio continuum data to derive the densities, masses, ionization requirements, and structural properties of a representative sample of the largest H II regions in nearby spiral and irregular galaxies. In addition, published radio continuum maps of several Galactic H II regions, including the largest known objects, have been analyzed in the same way, in order to directly compare the Galactic and extragalactic populations. In this paper I shall concentrate on the structural properties of a small sample of nearby objects, in order to provide a homogeneous set of data on the properties of giant H II regions and to illustrate the diversity in both their structures and their integrated properties. Later papers will deal with the statistical properties of the H II region populations in different types of galaxies.

¹ Visiting Astronomer, Kitt Peak National Observatory, National Optical Astronomical Observatories, operated by the Association of Universities for Research in Astronomy, Inc., under contract with the National Science Foundation. Visiting Astronomer, Cerro Tololo Inter-American Observatory, National Optical Astronomical Observatories, operated by the Association of Universities for Research in Astronomy, Inc., under contract with the National Science Foundation. Guest Investigator, Palomar Observatory, which is operated by the California Institute of Technology.

II. DATA

a) Extragalactic H II Regions

Photoelectrically calibrated H α emission maps were obtained for the largest H II regions in the LMC, the SMC, M31, M33, NGC 6822, IC 1613, NGC 2366, M81, NGC 2403, M82, and M101. Local Group objects were preferentially selected to maximize spatial resolution and to minimize the confusion between large single H II regions and close clusters of small regions. A few unusual types of regions are not found in the Local Group, most notably the very bright regions that are often found in Markarian galaxies, and the compact clusters of giant H II regions that often occur in large Sc galaxies. Examples of these objects have been taken from NGC 2366, M82, and M101. Table 1 lists the H II regions, and several objects are illustrated, on the same absolute linear scale, in Figure 1. For each galaxy I selected the brightest H II region and sometimes one or two others, especially if the latter exhibited a significantly different structure. As will be discussed later, the largest H II regions in most galaxies tend to be similar, so the objects listed in Table 1 are usually representative examples, at least in terms of their surface brightness, density, and structure. Exceptions, such as the 30 Doradus nebula in the LMC, are noted as such in the table.

For each galaxy, calibrated H α interference filter photographs were obtained, using the two-stage Carnegie image-tube camera on the Kitt Peak 2.1 m and 0.9 m telescopes (M33, M81, M101, NGC 2366, NGC 2403, NGC 6822, IC 1613), and direct cameras on the Palomar 1.2 m Schmidt Telescope (M31), and the Curtis Schmidt telescope at Cerro Tololo (LMC, SMC). Digital maps of individual H II regions were made with the PDS microdensitometer at Kitt Peak and were converted to relative-intensity maps using sensitometer exposures. The integrated H α emission-line flux of each H II region was measured, using single-channel photometers on the Kitt Peak 0.9 m, Cerro Tololo 0.6 m, and University of Washington Manas-

GIANT H II REGIONS

TABLE 1
THE H II REGION SAMPLE

Object	Other Names, ID's	Adopted Distance (kpc)	Angular Resolution ^a (arcsec)	Linear Resolution (pc)	Adopted $A(H\alpha)$ (mag)
Extragalactic H II Regions					
30 Doradus ^b	LMC N157, DEM 263	50	30	8	1.2
LMC N70	DEM 301	50	30	8	0.0
SMC A	N66, DEM 103	70	30	11	0.5
SMC B	N19, DEM 31	70	30	11	0.7
NGC 6822 A	Hubble X	600	3	9	0.7 ^c
NGC 6822 B	Hubble III	600	3	9	0.7 ^c
NGC 6822 C	Hubble V	600	3	9	1.2 ^c
M31 A	Pellet 550	680	3	10	1.2
M31 B	Pellet 281	680	3	10	1.2
M31 C	Pellet 258	680	3	10	1.2
M33 A	NGC 604	800	3	12	0.7
M33 B	NGC 595	800	3	12	1.2
M33 C	NGC 592	800	3	12	1.0
IC 1613 A	Baade 10	800	2	8	0.0
IC 1613 B	Baade 15/16	800	2	8	0.0
IC 1613 C	Baade 3	800	2	8	0.0
NGC 2366 A ^b	NGC 2363, Mrk 71	3500	2	35	0.4
NGC 2403 A	VS 44	3500	2	35	1.0
M81 A	Hodge 42	3500	2	35	1.2
M82 A	...	3500	2	35	2.5;
M82 B	...	3500	2	35	2.5;
M101 A	NGC 5471	6000	1	30	1.2
M101 B	NGC 5461	6000	2	60	1.7
M101 C	NGC 5455	6000	2	60	1.2
Comparison Galactic H II Regions					
Orion	NGC 1976, Orion A	0.5	120	0.3	...
M8	NGC 6523, Lagoon nebula	1.4	240	1.6	...
NGC 224	Rosette nebula	1.4	180	1.2	...
Carina	NGC 3372, RCW 53	1.4	240	3	...
NGC 3603	RCW 57	8.5	240	10	...
W49	G43.2+0.0	14.1	370	25	...

^a Resolution for extragalactic regions is FWHM seeing, except for the Magellanic Cloud objects, where it is the sampling cell size. For Galactic regions the quoted resolution is the half-power beamwidth of the radio map used.

^b Unusually bright and large compared to any other H II region in the galaxy.

^c Most of the extinction is Galactic foreground.

tash Ridge 0.8 m telescopes, and with the SIT Vidicon camera on the Palomar 1.5 m telescope. These fluxes defined the calibration of the $H\alpha$ emission scales for each photographic map. For M82, the Palomar Vidicon camera was used directly to map the H II regions, with a scale calibration from the spectrophotometry of O'Connell and Mangano (1978). Most of the data used here were obtained earlier as part of a study of H II regions as distance indicators (Kennicutt 1979), and details of the reduction and calibration procedures may be found there.

The extinction can be substantial in many of these H II regions, and it is important to correct at least approximately for its effects. Radio fluxes compiled by Israel and Kennicutt (1980), Klein, Grave, and Wielebinski (1983), and Walterbos and Schwing (1984) were combined with the $H\alpha$ fluxes in this paper to derive the optical extinction for each H II region, using the free-free emissivity as computed by Oster (1961). These integrated extinction values are listed in Table 1. While variations in extinction across a few giant H II regions have been reported (e.g., Israel *et al.* 1982; Viallefond, Donas, and Goss 1983; Fitzpatrick and Savage 1983), the poor resolution of the radio data only allows us to make an average extinction

correction for each object. To test the reliability of this procedure, mean emission measure and rms electron density profiles were derived for the 30 Doradus H II region in two ways: using the $H\alpha$ emission distribution (corrected uniformly for extinction as described above), and with the 6 cm radio continuum map of Mills, Turtle, and Watkinson (1978). The results of each model are compared in Figure 2. If the 30 Doradus results are representative, the Balmer-line maps should be quite adequate for studying the large-scale structure of the giant H II regions, provided that an average correction for dust is applied.

While this crude extinction correction appears to be valid over relatively large areas in the bright central regions, it is possible that the extinction is considerably lower in the diffuse outer halos of the H II regions (Koorneef 1978). Since the available radio maps generally cover only the bright central regions (in Fig. 2, for example, the radio measurements cover only the central half-radius of 30 Doradus), applying this central extinction correction to the H II regions as a whole probably would result in an overestimate of the total nebular luminosities and ionization requirements. I have attempted to take this effect into account when adopting the mean extinction values listed

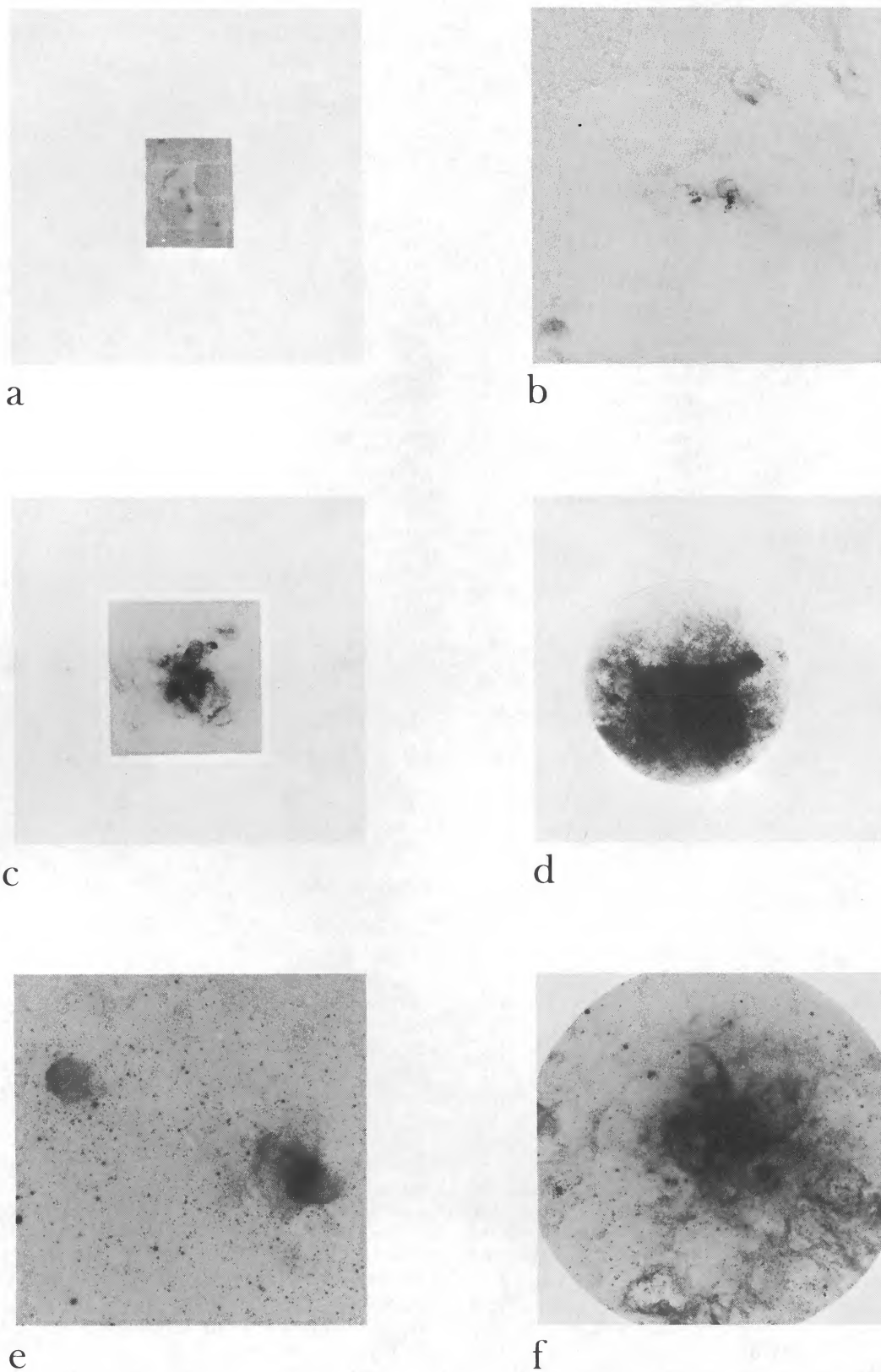
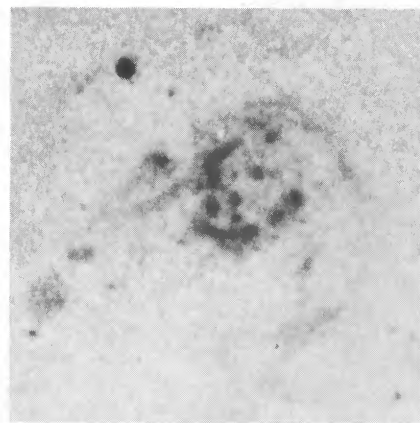
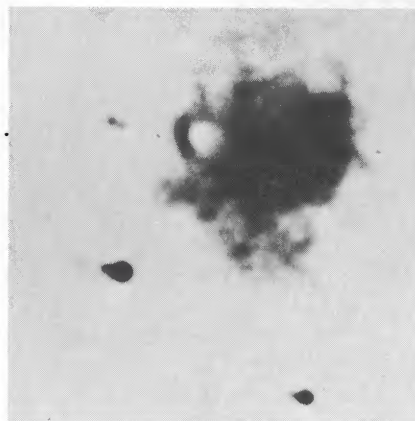


FIG. 1.— $H\alpha$ -bandpass photographs for some of the $H\ II$ regions in this study. The photographs have been enlarged to the same physical scale, 600 pc on each full panel side. (a) The constellation of Orion, including the Orion Nebula and the Barnard Loop. Composite Palomar Sky Survey red photograph. (b) NGC 3603, illustrating the severe obscuration problem for distant Galactic objects. (c, d) The Carina nebula, NGC 3372. The left-hand panel is a $1\frac{1}{2}$ hour Curtis Schmidt exposure, while the right-hand panel is the same region photographed with a two-stage image tube, from Parker, Gull, and Kirschner (1979). The latter exposure is representative of how NGC 3372 would appear if photographed from a nearby galaxy using the techniques described in this paper. (e) $H\ II$ regions Henize N66 and N76 in the SMC. (f) 30 Doradus in the LMC.



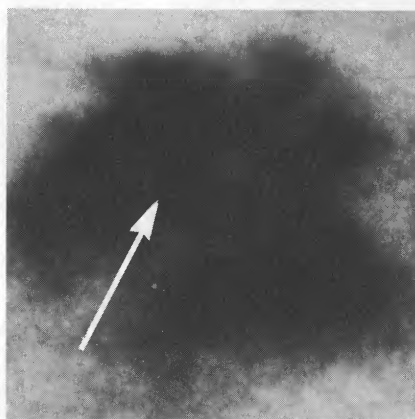
g



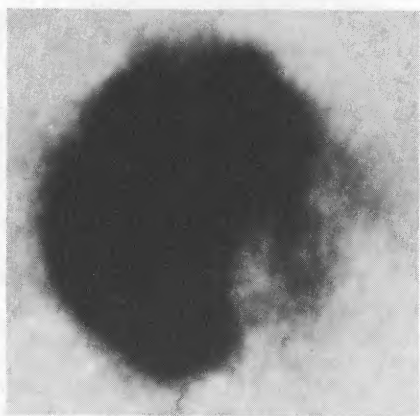
h



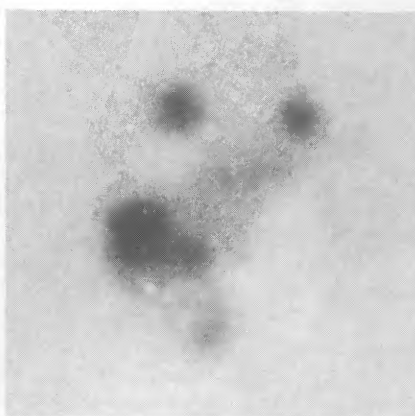
i



j



k



l

FIG. 1 (Continued).—(g) Pellet 550, one of the largest H II regions in M31. (h) NGC 604, the largest H II region in M33. (i) Henize N70 in the LMC, a prototype ringlike region. (j) The central region of M82. The arrow denotes the position of M82 A. Note that this exposure is an order of magnitude shorter than the others. (k, l) NGC 5471, the largest H II region complex in M101, long and short exposures showing the outer and inner structures.

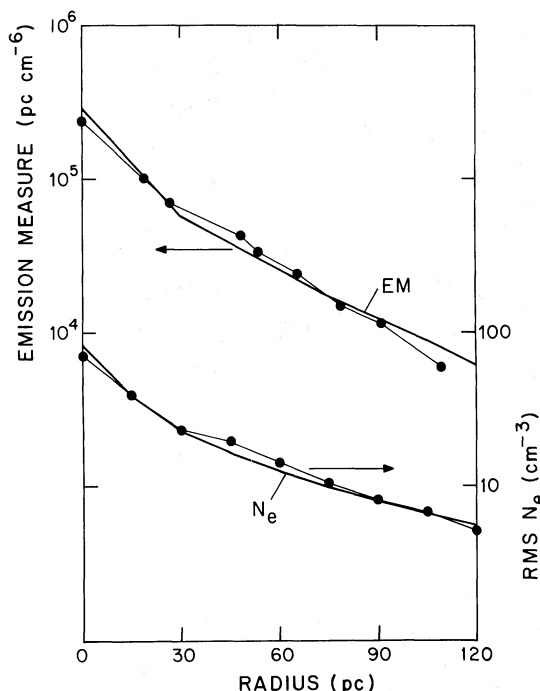


FIG. 2.—A comparison of H α -derived and radio continuum-derived emission-measure profiles (*upper curves*) and electron density profiles (*lower curves*) for 30 Doradus. The solid line represents the H α data, scaled by a constant absorption correction factor. The points joined by the light line are the corresponding radio-derived parameters.

in Table 1. The reader should also be aware that the emission profiles presented later in this paper may be affected by a small radial extinction gradient.

b) Galactic H II Regions

For Galactic objects H α maps are less useful, because heavy nonuniform foreground extinction often severely obscures the true nebular structure. Figure 1*b* shows an example of the severity of this effect, in NGC 3603. As a consequence, published radio continuum maps were used directly for the Galactic objects. The angular resolutions of optical maps for a typical Local Group galaxy and single-dish maps of typical Galactic H II regions correspond to nearly identical physical scales (~ 5 –20 pc), enabling us to compare optimally the two sets of objects. The only drawback of the radio maps is their significantly lower sensitivity to faint extended emission (the limiting emission measures are typically an order of magnitude higher). In the analysis which follows, I have compensated for this difference either by extrapolating the radio profiles using H α data or by restricting the comparisons of Galactic and extragalactic objects to the high surface brightness regions as described later.

Published radio maps are available for several hundred Galactic H II regions. For this analysis six representative objects were selected, including three well-known objects, Orion, M8, and the Rosette nebula NGC 2244, as well as three H II regions which are generally considered to be among the largest and brightest in the Galaxy, the Carina complex (NGC 3372), NGC 3603, and the W49 complex. Single-dish continuum maps of these regions were taken from several sources and are listed in Table 1. Spectroscopic distances were used for all objects except W49; for W49 the kinematic distance derived by

Mezger, Schraml, and Terzian (1967) was adopted. The radio maps themselves are from Mezger and Henderson (1967); Mezger, Schraml, and Terzian (1967); Schraml and Mezger (1969); Goss and Shaver (1970); Gardner *et al.* (1970); and Celnick (1983).

III. ANALYSIS

a) Mass Models

Simple spherically symmetric mass models were constructed for 23 representative H II regions, in order to derive approximate electron density distributions. The observed H α surface brightnesses were converted to emission measures using the case B recombination rate of Brocklehurst (1971). The radio brightness temperature maps were converted to emission measures (EM) using the emissivities from Oster (1961). In both cases an average electron temperature of 10,000 K was assumed, except for NGC 2366 A, where 15,000 K was used (Kennicutt, Balick, and Heckman 1980). The emission measure distribution in each object was then azimuthally averaged to derive a mean radial profile. This profile was truncated at EM = 300 pc cm $^{-6}$ in order to avoid confusion with diffuse galactic emission. The radio measurements are less sensitive, with limiting emission measures of 1000–5000 pc cm $^{-6}$. In order to account roughly for the diffuse emission beyond those radii, the radio profiles were extrapolated to EM = 300, but in most comparisons of the Galactic and extragalactic objects we will restrict our attention to the bright regions (EM > 10 3). Any results affected by extrapolation will be noted as such in the analysis that follows.

The emission measures in the H II regions studied here cover a very broad range, from less than 10 3 in the brightest parts of some of the diffuse extragalactic regions to 10 6 or more in the cores of the Galactic objects. The EM distributions cover a broad range as well, from bright centrally condensed objects to diffuse rings and shells. Radial emission-measure profiles for the first-ranked H II regions in three Local Group galaxies are illustrated in Figure 3, and photographs of several others are illustrated in Figure 1.

A spherically symmetric shell model has been used to derive the approximate radial distribution of electron density from the emission-measure profile:

$$EM(x) = 2 \int_x^R \frac{0.92rN_e^2(r)}{(r^2 - x^2)^{1/2}} dr,$$

where x is the projected radial coordinate in the plane of the sky, r is the true radial coordinate within an H II region of radius R , and the constant corrects for electrons from helium. While this spherical approximation is clearly unrealistic in detail, it will serve to yield the approximate distribution of (rms) density within the H II regions. The Abelian integral was solved numerically by dividing each region into shells (10–30, depending on the resolution and continuity in the EM profile), and integrating inward from the outer shell. Examples of rms density profiles derived in this way are shown in Figures 6, 7, 8, and 10. Before we use these densities to estimate the nebular masses, however, the effects of clumping must be considered.

b) Forbidden-Line Densities and Filling Factors

On small scales the H II regions are extremely inhomogeneous. Optical filaments dominate the structure of nearby objects such as 30 Doradus (see Fig. 1), and detailed studies of Galactic objects (e.g., Osterbrock and Flather 1959) reveal

clumping on yet smaller scales. It is essential that we estimate the degree of clumping and to correct approximately for its effects in deriving the nebular masses. For simplicity the regions were assumed to contain two components, high-density clumps occupying a fraction δ of the total volume and a low-density interclump medium assumed to contribute negligibly to the total emission or mass. In such a simple case the clump density and the rms density are related by the square root of the filling factor. Published spectrophotometry of the [S II] $\lambda\lambda 6717, 6731$ and [O II] $\lambda\lambda 3727, 3729$ forbidden lines was compiled for all available objects and used to derive electron densities in the high-density clumps. These in turn were compared with the rms densities derived for the same parts of the H II regions (almost always the central cores) and used to estimate the volume filling factor δ .

Reliable forbidden-line densities are available for 12 of the H II regions in Table 1, and they are compared with the corresponding rms densities in Figure 4. Both sets suffer from considerable uncertainties in individual objects. The [S II] and [O II] densities often fall near the asymptotic low-collision limits ($N_e < 10^3 \text{ cm}^{-3}$), so that the derived values are often uncertain by factors of 2–5 (objects with [S II] ratios at the low-density limits were excluded from this analysis). The corresponding rms densities suffer from several uncertainties, extinction, resolution effects, and error due to projection effects along the line of sight to the center; they are probably good only to within a factor of 2–3.

The filling factors of most of the H II regions shown in Figure 4 fall within the range $10^{-2} < \delta < 10^{-1}$, perhaps a surprisingly narrow range considering the 3-order-of-magnitude density range and the quadratic sensitivity of δ to errors in the densities. One H II region, M82 A, falls well outside this range. This may be due to a large underestimate of the extinction (no

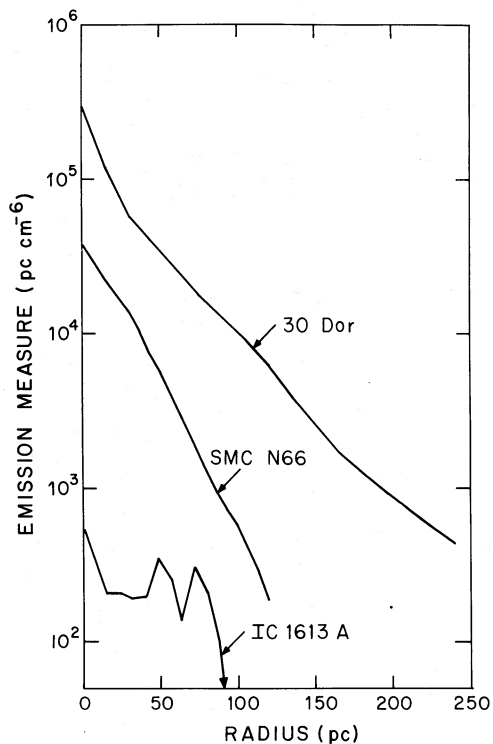


FIG. 3.—Examples of azimuthally averaged emission-measure profiles for three first-ranked extragalactic H II regions.

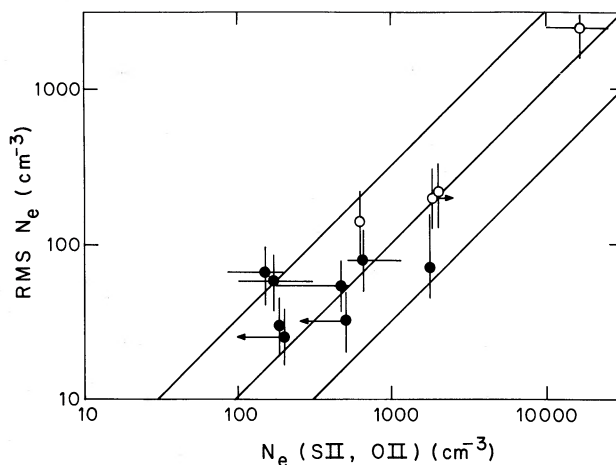


FIG. 4.—Comparison of central rms electron densities derived from the absorption-corrected $H\alpha$ photometry, and corresponding forbidden-line densities from published [O II] and [S II] measurements. Lines of constant volume filling factor are also shown.

radio data are available), but it could also reflect the highly peculiar nature of this object (O'Connell and Mangano 1978), as discussed later. The results in Figure 4 show that while the giant extragalactic H II regions possess characteristic sizes and densities that often differ markedly from smaller Galactic H II regions, their small-scale geometries are similar. Most of the volume in the giant H II regions is occupied by a very low density medium ($n_e \ll 1 \text{ cm}^{-3}$). It is important to note, however, that we have adopted a relatively simple model, in which the filling factor measured at a single point (usually the center) has been applied for the nebula as a whole. A more detailed analysis (O'Dell and Castenada 1984) suggests that the filling factor itself may vary considerably within individual regions. The nebular densities and masses derived here should be treated as reasonable estimates, useful for comparative purposes, but detailed mapping of the [O II] ratio across an individual H II region will be necessary before an accurate picture of the internal density structure can be obtained.

c) Integrated Properties

Table 2 provides a summary of the primary integrated properties of the six Galactic and 24 extragalactic H II regions studied here. The emission measures, luminosities, rms densities, and filling factors have been discussed already. Table 2 also lists approximate diameters, masses, and ionization requirements.

The diameters listed in the table correspond to the outer limits seen from visual inspection of the $H\alpha$ photographs, and as such are intended only as rough indicators of size. In as diverse a sample of objects as this one, there is no single physically meaningful diameter (Kennicutt 1979); many of these objects do not even possess physical edges, but an approximate visual diameter is useful for comparative purposes. The corresponding diameters of many of the Galactic H II regions can be only crudely estimated, because of foreground extinction and confusion with unassociated emission nebulosity along the line of sight. This point is illustrated in Figure 1. Figure 1b shows a deep $H\alpha$ -bandpass exposure of the NGC 3603 region. Virtually all of the nebulosity is obscured (the projected diameter of the radio emitting region is at least 100 pc), and much of what is visible in the field is actually unassociated nebulosity which is several kiloparsecs nearer than NGC 3603 (e.g., Goss and Ra-

TABLE 2
SUMMARY OF INTEGRATED PROPERTIES

Object	Type ^a	Diameter (pc)	Peak EM ^b (pc cm ⁻⁶)	$L(H\alpha)$ (ergs s ⁻¹)	Average $\langle N_e \rangle_{rms}$ (cm ⁻³)	Peak $\langle N_e \rangle_{rms}$ (cm ⁻³)	Filling Factor δ	$M(H^+)$ (M_\odot)	$\log N_c$ (s ⁻¹)	Equiv. $N(O5 V)$	$M^*(OB)$ (M_\odot)
Orion	C	5	1.6×10^6	1×10^{37}	150	1600:	0.027	50	48.85	(0.2)	35
M8	C	25	2.5×10^5	3×10^{37}	60	220	0.012	900	49.35	(0.5)	100
NGC 2244	C-S	50	10000	8×10^{37}	13	20	(0.02)	2000	49.80	1	250
Carina	C-H	200:	3×10^5	6×10^{38}	13	140	0.05	44000	50.65	9	2000
NGC 3603	H	100:	$> 5 \times 10^5$	1.5×10^{39}	25	200:	(0.02)	39000	51.05	20	5000
W49	H	150:	$> 2.5 \times 10^5$	2×10^{39}	15	300:	(0.02)	45000	51.20	27	7000
LMC N70	S	110	2000	5×10^{37}	2	8:	(0.02)	7000	49.55	1	180
IC 1613 A	S	180	600	5×10^{37}	1.3	4	(0.02)	12500	49.55	1	170
IC 1613 B	S	170	400	3.5×10^{37}	1.2	49.40	(0.6)	120
IC 1613 C	S	110	1100	1.7×10^{37}	1	49.10	(0.3)	60
NGC 6822 B	S-D	200	500	2×10^{38}	1.7	2	(0.02)	19000	50.15	3	600
NGC 6822 A	D	160	13000	4×10^{38}	5	20	(0.02)	23000	50.50	6	1300
NGC 6822 C	D-H	130	60000	7.5×10^{38}	8	50.75	12	2500
SMC N19	D	220	4000	2.2×10^{38}	2.3	6	(0.02)	55000	50.20	3	700
SMC N66	D-H	220	30000	6×10^{38}	4	30	(0.02)	82000	50.65	9	2000
M31 A	S, M, D	250	1000:	5×10^{38}	3	20	(0.02)	46000	50.55	7	1700
M31 B	S, M, D	240	1200:	5×10^{38}	3	10	(0.02)	39000	50.55	7	1700
M31 C	D	190	1500:	4×10^{38}	4	20	(0.02)	15000	50.50	6	1300
M33 C (N592)	M, D-H	360	12000	3×10^{38}	1	50.35	5	1000
M33 B (N595)	H	400	40000	2.3×10^{39}	3	51.20	30	7000
M33 A (N604)	H	400	1.4×10^5	4.5×10^{39}	4	65	0.1:	7×10^5	51.50	65	15000
M81 A	D-H	450	15000	1.7×10^{39}	2	13	(0.02)	4×10^5	51.10	25	5700
30 Doradus	H	370	3×10^5	1.5×10^{40}	6	80	0.013	6×10^5	52.05	230	50000
NGC 2366 A	H	560	1.5×10^5	1.5×10^{40}	4	50	0.010	8.5×10^5	52.05	230	50000
NGC 2403 A	H, M	600	80000:	1.4×10^{40}	4	27	(0.02)	5.5×10^5	52.00	210	45000
M82 A	H	450:	6×10^5	4×10^{40}	16:	70:	$\geq .00015$	$\geq 2.5 \times 10^5$	52.45:	600:	1.3×10^5
M82 B	H	300:	4×10^5	3×10^{40}	15:	52.35:	450:	1.0×10^5
M101 A (N5471)	M, H	800	2×10^5	5×10^{40}	4	60	0.09	9×10^6	52.55	750	1.7×10^5
M101 B (N5461)	(M), H	1000:	2×10^5	7×10^{40}	3.5	30:	0.02	6×10^6	52.70	1000	2.3×10^5
M101 C (N5455)	H	750	1.8×10^5	2.5×10^{40}	3	52.25	380	90000

^a C = classical, H = high surface brightness giant H II region, D = diffuse giant H II region, M = multiple core complex, S = shells or ringlike H II regions.

^b These values may be affected by resolution.

dhakrishnan 1969). In the case of NGC 3603 and the even more heavily obscured W49 complex, I have very crudely estimated an "optical" diameter by extrapolating the radio continuum contours to an isophote corresponding to $EM = 10^3$, which very roughly corresponds to the visual limit in moderately exposed $H\alpha$ photographs (Kennicutt 1979). Figures 1c–1d illustrate another example, the Carina region around η Carinae and NGC 3372. Figure 1c is a $1\frac{1}{2}$ hour $H\alpha$ -bandpass Schmidt camera exposure, showing the extent of the nebula which appears in most photographs of the region. A much deeper image-tube exposure in $H\alpha$, however, shown in Figure 1d, reveals faint nebulosity extending over a region about 300 pc in diameter (photograph from Parker, Gull, and Kirschner 1979). If all of this nebulosity is associated with NGC 3372 (again the line of sight passes nearly along the Carina spiral arm), then the H II region is comparable in size to the large extragalactic giant H II regions. This example illustrates the severity of the observational bias encountered when one attempts to compare Galactic and extragalactic regions in an unbiased manner.

The mass of ionized gas in each region was estimated by integrating the rms density distribution and correcting this rms mass by the square root of the central filling factor. (For H II regions with no reliably measured filling factor a mean value $\delta = 0.02$ was assumed.) Finally, three indications of the stellar ionization are listed: the Lyman continuum photon luminosity derived from the extinction-corrected $H\alpha$ flux and the recombination ratios from Brocklehurst (1971); the equivalent number of O5 V stars, assuming $N_L(\text{O5 V}) = 5 \times 10^{49} \text{ s}^{-1}$ (Panagia 1973); and the total stellar mass in the range 10–100 M_\odot , assuming solar-composition stars following a Salpeter initial mass function. The latter ionization model is from Kennicutt (1983), and the quoted stellar mass is for stars above 10 M_\odot only, since stars below that limit do not contribute significantly to the ionization. These ionization requirements are strictly only lower limits, of course, since it is possible that some of the H II regions may not be radiation-bounded. The emission spectra of most large, bright H II regions in late-type spirals are best represented by radiation-bounded models (McCall 1982), and in the following analysis I shall implicitly assume that this is generally the case; but it should be noted that specific objects, especially the ringlike H II regions, may be density-bounded.

A casual inspection of Table 2 reveals that the extragalactic H II regions span an enormous range in physical properties, but a few general patterns can be seen. Overall we are dealing with objects which are larger, brighter, and less dense than most familiar Galactic H II regions. A small part of the difference may be due to observational selection; the $H\alpha$ surveys of external galaxies are sensitive to fainter emission measures (and hence lower densities) than most Galactic surveys, but as will be discussed in § V most of the discrepancy is real. The tendency for the giant H II regions to possess lower average electron densities is actually an extension of a trend seen in Galactic H II regions, as first pointed out by Israel (1976). Figure 5, adapted from Habing and Israel (1979), shows the relation between average rms density and diameter for ~ 100 Galactic H II regions (or components) observed with the Westerbork radio telescope, along with the corresponding properties of the H II regions measured in this paper. A plot of nebular density versus luminosity (not shown) shows a similar behavior. Israel (1976) and Habing and Israel (1979) interpret the relation for the compact regions as being an evolutionary sequence. For the largest objects, including the H II regions

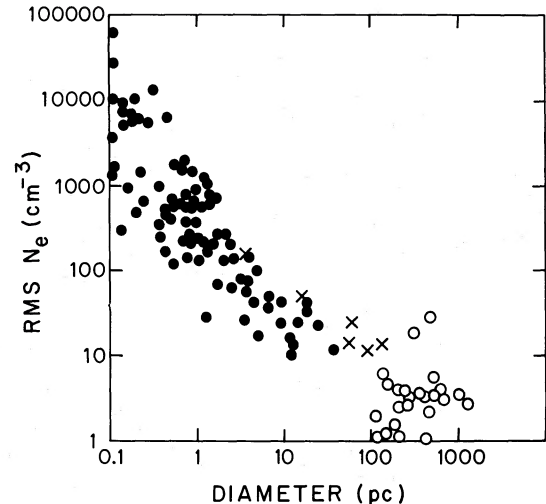


FIG. 5.—Relationship between volume-averaged rms electron density and H II region diameter for Galactic and extragalactic H II regions. Open circles are extragalactic H II regions studied in this paper, crosses are Galactic regions studied here, and filled circles are Galactic H II regions and H II region components measured by Israel (1976).

studied in this paper, the explanation must be different. The rms densities in the envelopes of the giant H II regions are of the same order as the average (total) interstellar densities in galaxies ($\sim 1 \text{ cm}^{-3}$), so perhaps the ultraviolet luminosities of the stars in the giant H II regions are so large that they have ionized not only the dense cores in which they formed but an extended volume of the surrounding interstellar medium.

Among the extragalactic objects themselves, there is a three-order-of-magnitude range in luminosity and mass. While there is a considerable overlap in size and luminosity between the Galactic and the extragalactic objects, the two groups are distinct in most cases in terms of their density and structure. The largest extragalactic objects surveyed here are unparalleled in the Galaxy, with massive stellar contents which often surpass the integrated contents of entire galaxies (cf. Kennicutt and Kent 1983).

IV. DISCUSSION: THE EXTRAGALACTIC H II REGIONS

There is no such thing as a single prototypical giant H II region. The diversity in the properties of the extragalactic H II regions is as pronounced as any systematic difference between those objects and the "normal" Galactic regions. Moreover, it is a mistake to regard the extragalactic H II regions as simply a one-parameter extension to the luminosity function of the Galactic regions, or as composite clusters of small Galactic-sized H II regions. The giant H II regions comprise *at least* a two-parameter family. The luminosities and densities of the largest H II regions in different galaxies vary widely and independently, although the objects in any one galaxy are often surprisingly similar.

Before discussing these general results in more detail, it is important to consider the properties of individual H II regions. To do this I have found it convenient to classify the giant H II regions into several broad groups. This classification is probably incomplete and of limited physical significance, and should not be overinterpreted. It does, however, provide a useful means of defining the systematic trends that are observed in the H II regions. The reader should be aware that with the exception of the classical H II regions below, all of the

other classes have been referred to in the literature at one time or another as "giant" or "supergiant" H II regions.

a) *Classical H II Regions (Orion, M8)*

Objects like Orion or M8 are almost certainly present in most spiral galaxies, but their small sizes and low luminosities make them difficult to isolate and study as such in all but the nearest external galaxies. I shall defer a detailed comparison of the classical Galactic and the extragalactic H II regions to the next section. The class is included here simply for completeness, as a reminder that the absence of such objects in extragalactic studies is almost entirely an observational selection effect.

b) *High Surface Brightness Giant H II Regions*

This is a prevalent type of H II region in late-type spiral galaxies, and the type most often studied in spectrophotometric surveys and the like. Giant spirals such as M101 may contain dozens of such objects, while low-luminosity galaxies or early-type spirals (Sa-Sb) rarely contain more than one or two, if any at all (Kennicutt 1984). Figures 6 and 7 show rms electron density profiles for the two nearest extragalactic regions of this type, 30 Doradus in the LMC, and NGC 604 in M33. This type of H II region is characterized by a centrally condensed density distribution, although the central (rms) densities ($10\text{--}100\text{ cm}^{-3}$) are generally 1–2 orders of magnitude lower than the typical central densities in the compact Galactic H II regions. Part of this difference may be a resolution effect; if compact (of the order of 1 pc or less), very dense components were present, they could easily be smeared out in the rms density profiles. Most of the difference is real, however. As shown in Figure 4, the central forbidden-line densities are also lower in the extragalactic objects. If high-density regions occupied a significant fraction of the central nebular volume, they would dominate the [S II] and [O II] ratios. (The forbidden-line measurements are also subject to resolution

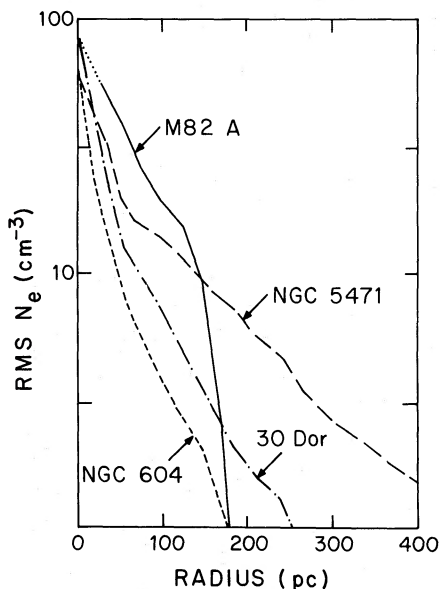


FIG. 6.—Approximate rms electron density profiles for four giant extragalactic H II regions. A spherically symmetric model has been assumed in deriving these profiles. For NGC 5471 and M82 A the inner 50 pc are uncertain because of resolution limitations. The falloff at large radii in M82 A could be artificial as well, because of the bright complex background in M82.

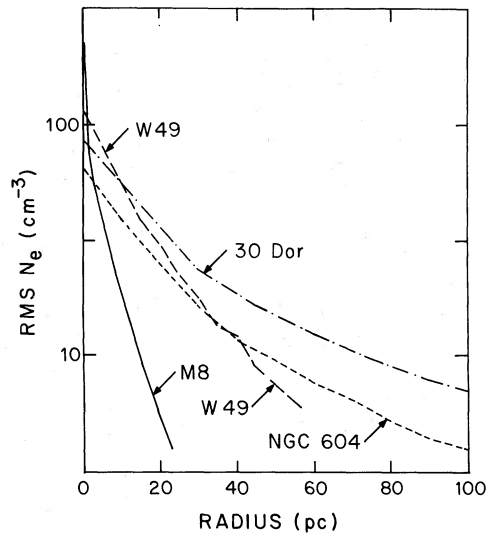


FIG. 7.—Central rms electron density profiles for 30 Doradus and NGC 604, as described in Fig. 6, along with profiles for two Galactic H II regions.

effects to some degree, of course.) Thus while Orion-like condensations may be present, and are indeed likely to be present in many of the high surface brightness H II regions, the bulk of the emission, even at the centers, arises from much lower density gas in most cases. (In the diffuse H II regions that predominate in low-luminosity galaxies, there is no evidence for any dense material at all.) Outside the core there is usually a steep radial density gradient in the H II regions; most of the nebular mass is composed of relatively diffuse, interstellar-density gas. Thus, while there is no evidence in these results for a distinct core-halo structure (Sandage and Tammann 1974; Israel 1976), the density profiles are consistent with a simple model in which these H II regions are relatively compact condensations that blend smoothly with the underlying interstellar medium.

The ionization requirements of these objects are generally large ($N_L > 10^{50}\text{ s}^{-1}$); they must be ionized by large clusters of "normal" ($M \lesssim 100 M_\odot$) OB stars or by objects with masses considerably greater than the commonly accepted stellar stability limit. The largest objects of this type (e.g., 30 Doradus) are most impressive indeed, with diameters in excess of 500 pc and luminosities requiring the ionization of several dozen normal O-type stars. Several investigators have created a separate class of supergiant H II regions to describe them. As will be discussed later, however, it is not clear that this distinction is physically meaningful.

The central cores (inner 50 pc) of these extragalactic H II regions are surprisingly similar in structure to the largest Galactic objects, as illustrated in Figure 7. Two Galactic regions in particular, NGC 3603 and W49, possess density profiles that are nearly identical with the giant H II region NGC 604, the largest and brightest H II region in M33. It is not known whether either NGC 3603 or W49 is nearly as large as the typical extragalactic objects, although they certainly extend well beyond the limits shown in Figure 7. The brightest Galactic H II regions may be comparable to many extragalactic objects which have traditionally been called "giant" H II regions, although there are almost certainly no Galactic analogs to the largest regions of this type. NGC 3603, for example, is still nearly an order of magnitude fainter than 30

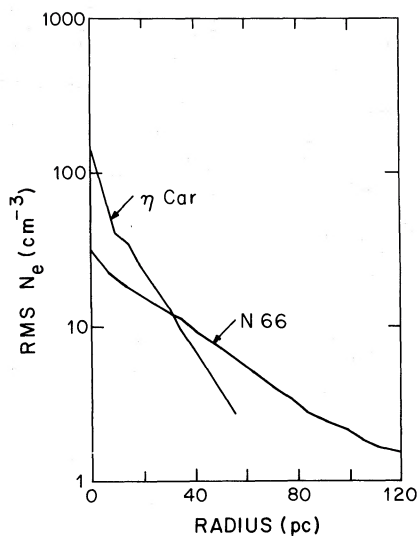


FIG. 8.—Comparison of rms electron density profiles of the Carina nebula, one of the brightest Galactic H II regions, and N66, the first-ranked region in the SMC. Note that these regions possess nearly identical total luminosities.

Doradus, and hence comparisons of either the gaseous or the stellar contents of NGC 3603 and 30 Doradus should not be made indiscriminately.

c) Diffuse Giant H II Regions

Most of the late-type galaxies studied here possess a large number of H II regions with luminosities that are comparable to the brightest Galactic regions, but with a much more diffuse and extended structure. The point is illustrated in Figure 8, which compares the rms density profiles of the brightest H II region in the SMC (N66) and the η Carina nebula. While the brightest H II regions in the SMC and the Galaxy possess comparable emission-line luminosities, the structures of the surrounding H II regions themselves are totally different. This is clearly not a result of small-number statistics or observational selection. Low-luminosity irregulars such as the SMC and NGC 6822 possess only the extended diffuse H II regions and the shell-like objects discussed below; the bright, compact Carina-type H II regions are not present. The point is illustrated in Figure 9, which shows an H α -bandpass photograph of the SMC. More luminous galaxies such as M33 or the LMC possess both high surface brightness and diffuse regions, as well as the shell-type objects discussed below. It is important to remember that the H II region types defined here are not as much physically distinct objects as extremes in what is actually a continuous sequence of nebular luminosities, densities, and morphologies.

While Galactic analogs to this type of H II region were not included in this study, such objects certainly exist in the Galaxy, at least on smaller scales. The North American nebula NGC 7000 is a good example. Very large objects like those in the SMC and NGC 6822 would be relatively easy to overlook in existing radio or optical surveys of the Galactic plane, unless they were very near by.

d) Shells

Ringlike H II regions are found in all of the galaxies studied, especially in low-luminosity irregulars and in the outer disks of spirals (see Figs. 1 and 8). They appear to be similar to the Galactic ring nebulae discussed by Gum and de Vaucouleurs

(1953) and especially the Magellanic Cloud rings, which have been studied in detail by Lasker (1977, 1979), Meaburn (1980), and Chu (1982, 1983). The examples discussed here are relatively small ($D < 200$ pc), round regions associated with young stellar associations. A few galaxies are also known to possess networks of long, complex filaments and loops, which are often called shells or supershells as well (e.g., Meaburn 1979). Since these latter emission regions appear to be distinct in many ways from ordinary H II regions, they will be discussed only briefly at the end of this section.

Figure 10 shows the radial rms density profiles for NGC 6822 B and N70 in the LMC. A slightly different procedure was used to derive the N_e profiles in these objects. Because the shells are usually quite thin and noncircular, averaging the radial profiles would have introduced an artificial broadening of the shells. Instead, narrow radial cuts were made, in directions that were representative of the average structure. A spherical model was used in estimating the run of rms density, and in many instances small regions of imaginary electron densities were found, indicating a breakdown of this assumption in detail, as shown in Figure 10. The discrepancies are relatively small, however, and hence the derived nebular densities and masses are probably accurate at the factor-of-2 level. (It should be noted that in all of the ringlike regions studied here there is substantial emission within the ring itself, indicating the presence of material along the line of sight to the interior.)

The surface brightness in the rings is quite low, with the emission rarely exceeding 1000 pc cm^{-6} , and the derived rms densities in the shells are correspondingly low, of order $1\text{--}10 \text{ cm}^{-3}$ in most cases. This is partly a resolution effect; when high-spatial-resolution images are available (e.g., N70 in the LMC), the shells are often seen to resolve into narrow, bright filaments. In any case, the shell nebulae are the least massive and luminous of the "giant" H II regions, with H^+ masses of a few thousand solar masses, and ionization requirements that can be provided by a few single O stars (see Table 2).

While the ringlike regions occur in all of the nearby galaxies with sizable H II region populations, they are especially prevalent in low-luminosity irregulars and in the outer disks of spirals. Virtually all of the detected H II regions in IC 1613 are rings, for instance (see also Table 2), and they are the predominant type in the outer parts of M33 (Boulesteix *et al.* 1974). These are usually regions of low interstellar gas density and lower heavy element abundances, and there is some evidence that suggests that the structure and/or evolution of the H II regions have been influenced by the different environment; Boulesteix *et al.* (1974) point out that the average ring diameter rises sharply with increasing galactocentric radius in M33, and Braunsfurth and Feitzinger (1983) find evidence for a direct relationship between ring diameter and local gas density in the LMC. More detailed observations will be required to distinguish effects due to the ambient interstellar medium from differences, for example, in the masses and winds of the embedded stars.

The ringlike H II regions are most easily understood from a theoretical point of view as being an evolved stage of what was previously a diffuse amorphous H II region (e.g., Castor, McCray, and Weaver 1975; McKee, Van Buren, and Lazareff 1984). It is tempting to link the diffuse H II regions discussed earlier with the ringlike regions in an evolutionary sequence, and it is possible that some of the larger shells may be fossil counterparts to the diffuse H II regions in those galaxies. As



FIG. 9.— $H\alpha$ -bandpass photograph of the SMC, showing the preponderance of low surface brightness, diffuse $H\ II$ regions, and shell-type objects. This $H\ II$ region population is typical of irregular galaxies of this luminosity. The original plate is a 5 hr exposure on the Curtis Schmidt telescope, exposed through a $40\ \text{\AA}$ interference filter.

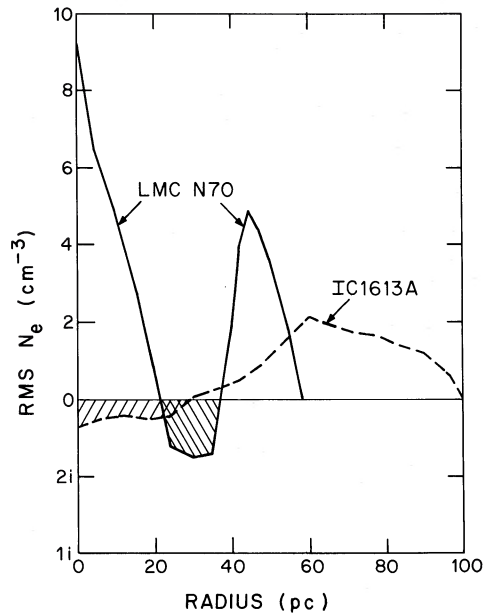


FIG. 10.—Approximate rms electron density profiles for two ringlike H II regions. Note the expanded linear scale. The crosshatched area denotes regions in which the spherically symmetric models yielded imaginary densities, indicating a breakdown of the spherical model in detail. In both cases, resolution effects have blended what are probably much narrower, higher density filaments.

discussed earlier, however, the rings often occur in regions where few if any other H II region types are detected. Where are the progenitors to the rings? I suspect that the less evolved H II regions are present, but they cannot be easily observed. In many galaxies the shells themselves are just barely detectable, with emission measures of only a few hundred. At earlier stages, before the gas has piled up, typical emission measures would be an order of magnitude lower and hence would be virtually undetectable in typical emission-line surveys. If this somewhat speculative picture is correct, a substantial fraction of the massive star formation in low-luminosity galaxies and the outer regions of spirals may be missed by conventional surveys of H II regions.

A substantial fraction of the emission regions cataloged in the Magellanic Clouds (Davies, Elliot, and Meaburn 1976) are large, complex filamentary structures, often extending over kiloparsec-sized regions. As part of this study, photometric scans were made through several of the LMC loops. The emission measures (typically 10^2 – 10^3 pc cm^{-6}) and thicknesses (10–100 pc) of the large loops are comparable to those in the smaller ring nebulae described earlier. The present data do not allow us to derive reliable estimates of the physical properties of the emission regions, however; the three-dimensional geometry is unknown (they could be shells or filaments, for example), and the assumption that the regions are conventional ionization-bounded photoionized H II regions is open to serious question. Rather than elaborate here, I refer the reader to detailed studies of individual filament systems (e.g., Caulet *et al.* 1982).

e) Supergiant H II Regions?

Several investigators have grouped the brightest extragalactic H II regions into a separate class; these objects may be referred to in the literature as “supergiant,” “hypergiant,” or

“jumbo” H II regions. The implication that these very luminous objects may be physically distinct from the smaller giant H II regions has contributed to a controversy over whether supermassive stars may reside within the largest objects. Are the supergiant H II regions themselves structurally different from their less luminous counterparts, or are all of the differences simply manifestations of their heftier ionization sources?

Figures 6 and 7 show the radial rms density structures of several giant H II regions, including 30 Doradus, the prototype “supergiant” region. NGC 2366 A, M82 A, and the multiple-core complexes in M101 were also compared. With the notable exception of M82 A, which will be discussed separately below, the central regions of the supergiant H II regions are indistinguishable from less luminous “normal” giant H II regions, such as NGC 604 or even large Galactic objects like W49. The supergiant complexes possess unusually extended, low-density envelopes which contribute a large fraction of the total H α luminosity and ionized gas mass, but this can be understood simply in terms of their larger ionizing photon fluxes; the embedded stars have ionized not only the central high-density cores but a large surrounding region as well. Thus it is probably the unusually large ionizing sources that give the supergiant H II regions their spectacular appearance, not anything extraordinary in the gas cloud itself, at least when compared to other centrally condensed H II regions. A similar comparison can be made of the kinematic properties of giant H II regions (Melnick 1977; Gallagher and Hunter 1983; Skillman and Balick 1984). Here the interpretation is more controversial, but the results do suggest that there is a relatively continuous increase in velocity dispersion with increasing nebular size. This again may reflect simply the response of the gas to differences in the properties of the embedded star clusters, and in any case there is little evidence for a discontinuity between the properties of supergiant and “normal giant” H II regions, as they have been defined here.

Even if the supergiant H II regions do not form a separate class in terms of their structural or kinematic properties, might they form a distinct class in terms of their photoionization requirements? A detailed discussion of the statistics of H II region luminosities in these galaxies is beyond the scope of this paper, but it is interesting to note a few general results. In luminous late-type spirals with large numbers of H II regions, there seems to be a continuous distribution of nebular sizes and luminosities, from the largest 30 Doradus-class complexes down to regions at least 100 times fainter (e.g., Kennicutt and Hodge 1980; van den Bergh 1981). Hence in these galaxies there is a continuity in both structure and scale between the brightest and the faintest detected H II regions. On the other hand, the supergiant objects are most noticeable when they appear alone in galaxies which otherwise possess only relatively faint H II regions—for example, in low-luminosity irregular galaxies (e.g., Hodge 1983). Hodge examined the statistics of the H II region diameters in 16 irregular galaxies, and showed that the observed number of supergiant regions was several times higher than would be expected from extrapolating the diameter functions of the fainter regions. On that basis, he argued that the largest regions are a physically distinct class, at least in these galaxies, and he suggested that the difference could be the presence of one or more supermassive stars (Savage *et al.* 1983; Massey and Hutchings 1983). This distinction between the high-luminosity and low-luminosity H II regions in irregulars does not necessarily require the existence of a new class of H II region or supermassive stars,

however. As discussed earlier, the majority of H II regions in low-luminosity irregulars are diffuse objects that are structurally different from the bright, centrally condensed H II regions which are generally observed in spirals. The occasional giant H II regions that do appear in these systems are physically distinct from the rest of the H II region population, both in their nebular structure and their photoionization requirements, but they are comparable to, if not identical with, the central condensed regions discussed earlier. The presence of a "supergiant" H II region in a low-luminosity irregular requires more than the formation of a single supermassive star; it requires the formation and collapse of an unusually large gas cloud (for these galaxies), independent of whether supermassive stars are present. These large regions are similar to if not identical with the H II regions that dominate large late-type spirals. The existing statistics on H II regions in galaxies probably are not directly relevant to the supermassive star controversy, one way or the other. More detailed observations (e.g., Skillman 1984) may provide better constraints.

While I can find little evidence in these results for the existence of a separate class of supergiant H II regions, the regions in the center of M82 are quite unique. An H α image of the region is shown in Figure 1; the photograph is overexposed, even though the exposure is roughly 10 times shorter than for most of the other images in Figure 1. The radial density structure of M82 A is shown in Figure 6. The values are systematically uncertain by as much as a factor of 2–3, mainly because of a very uncertain absorption correction (the region is not resolved on available radio maps because of the strong non-thermal emission in the galaxy). The extinction in front of M82 A is very high; O'Connell and Mangano (1978) derived $A_v = 2.5$ mag from the Balmer decrement, and this value is almost certainly a lower limit to the true absorption. With this correction M82 A and M82 B possess the highest surface brightness and electron densities of any objects studied here (this would be the case even if no absorption correction were applied). For a detailed discussion of this remarkable object, the reader is referred to O'Connell and Mangano (1978). While M82 A is almost certainly not the stellar nucleus of M82, its spectroscopic and kinematic properties are similar to a galactic nucleus. It exhibits velocity gradients in excess of 100 km s^{-1} , and it may contain a compact star cluster with a mass of at least $10^7 M_\odot$. According to O'Connell and Mangano (1978), several other knots in M82 are similar (including M82 B in Tables 1 and 2). Whether such objects are common in more distant galaxies is not easy to determine, because resolution effects will make it difficult to distinguish these compact regions from more normal giant H II regions.

f) Multiple H II Region Complexes

Giant spirals such as M101 often contain large H II region complexes with luminosities that are as much as an order of magnitude higher than 30 Doradus, but in most cases those objects are composites of several 30 Doradus-class H II regions, each separated by a few hundred parsecs. Photographs of one such object, NGC 5471 in M101, are shown in Figure 1, and its rms density distribution (along a radius passing through the brightest knot) is shown in Figure 6. There is no doubt that many if not most of these complexes are coherent associated structures, with the multiple cores surrounded by a single symmetric envelope of ionized and neutral gas (Viallefond, Allen, and Goss 1981).

While the total luminosities of these complexes usually

exceed those of large single objects like 30 Doradus, the characteristic brightness of the single components is usually of the same order as that of 30 Doradus (or less). This appears to be the case for the major complexes in M101 (NGC 5447, NGC 5455, NGC 5461, NGC 5462, NGC 5471) as well as for NGC 2366 A, a double-core object. It is tantalizing to suggest that the Lyman luminosity of the 30 Doradus core ($1\text{--}3 \times 10^{51}$ photons s^{-1}) represents a characteristic luminosity, or at least a crude upper bound, to the luminosities of the largest single ionizing objects, whether they are populous young star clusters or individual "stars," but there are not enough data available to take this hypothesis very seriously. While much larger and/or brighter H II regions have been reported in more distant galaxies (e.g., Benvenuti, Casini, and Heidmann 1979; Keel 1982), the relatively poor spatial resolution of those data (typically several hundred parsecs) does not allow us to distinguish whether we are observing single or multiple objects.

While composite regions are especially common among the largest giant H II regions, they are also common on smaller scales. NGC 592 in M33 is probably the best nearby example, and irregular galaxies such as NGC 4449 and the LMC contain a considerable number of such objects.

V. COMPARISON WITH GALACTIC H II REGIONS

The differences that are apparent between most well-studied Galactic H II regions and the majority of the extragalactic regions are partly real and partly a result of observational selection. In this section we consider both effects in more detail.

It is no surprise that objects like Orion or M8 are not well represented in external galaxies. At the distance of M31 or M33, Orion would have an angular diameter of $2''$ and a 6 cm radio flux of about $200 \mu\text{Jy}$. At the distance of M101 even the brightest Galactic regions are barely resolved. Detailed examination and photometry of the H II region populations in nearby systems such as the LMC (Kennicutt and Hodge, in preparation) shows that counterparts to the compact Galactic H II regions considered here are present, either singly or as parts of larger complexes. They are probably present in most or all of the galaxies, but they can be detected in only a few.

Most of the other types of extragalactic H II regions discussed in the previous section, including the typical giant H II regions, probably are present in the Galaxy. Interstellar obscuration and confusion/dynamic range limitations inhibit the detection of extended, low surface brightness nebulosities in optical and radio surveys, but deep surveys such as Sivan's (1974) H α study reveal several examples of low surface brightness H II regions. These same selection effects make it difficult to recognize bona fide giant H II regions in the Galaxy. NGC 3603 and W49 (and possibly Carina) are examples of Galactic regions whose inner 100 pc cores are indistinguishable from most giant extragalactic H II regions, such as the largest objects in M33. Unfortunately the available radio continuum maps do not extend below emission measures of $5000\text{--}10,000 \text{ pc cm}^{-6}$, so it is not known how large the Galactic candidates really are. It is likely, however, that the Galaxy contains at least several legitimate giant H II regions, even by extragalactic standards.

On the other hand, the apparent absence of very luminous 30 Doradus-class H II regions in the Galaxy is almost certainly real. To demonstrate this, I have plotted the emission-measure profiles of several bright Galactic and extragalactic H II regions in Figure 11, on the same absolute scale. (Resolution smearing is significant for the inner 20 pc of the M82 and M101

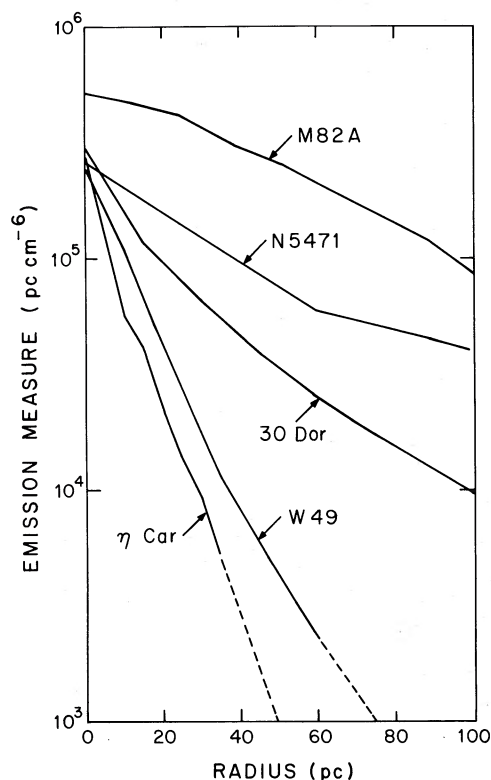


FIG. 11.—Azimuthally averaged emission-measure profiles for the inner regions of several Galactic and extragalactic H II regions. Since the emission measures are distance-independent projected surface brightnesses, this diagram illustrates the relative apparent brightnesses of the H II regions if they were placed at the same distance.

objects.) While the cores of Carina, NGC 3603, and W49 are comparable in brightness and extent to those in the extragalactic objects, most of the emission in the latter is coming from a much more extended region. This cannot be an observational selection effect; if Carina and NGC 3603 possessed extended regions that were comparable to those in the giant extragalactic H II regions, we almost certainly would have detected them.

Table 3 illustrates the point in another way. It shows what the approximate radio fluxes and angular diameters of several extragalactic H II regions would be if they were placed in the Galaxy at a distance of 5 kpc from the Sun. The diameter listed

TABLE 3
SOME H II REGIONS SCALED TO A COMMON DISTANCE OF 5 kpc

Object	Diameter (EM = 5000) (arcmin)	6 cm Radio Flux (Jy)
Orion	3	4
M8	14	10
Carina	50	200
NGC 3603	85	500
W49	60	650
30 Doradus	170	6000 ^a
M31 A	30	130 ^a
NGC 604	105	1700 ^a
M82 A	140	15000 ^a
NGC 5471	340	17000 ^a

^a These values refer to total source fluxes. Fluxes within the isophotal contour listed would be lower by as much as a factor of 2.

is an isophotal diameter, corresponding to an emission measure of 5000 pc cm^{-6} , roughly the limit of most Galactic surveys. For comparison I have also listed the corresponding numbers for the six Galactic H II regions, again scaled to a 5 kpc distance. It seems unlikely that many 3° diameter, 10,000 Jy sources would go unnoticed even if buried in the center of the Galactic plane. While a few objects on the scale of the largest in M33 may be present, the largest H II regions in the Galaxy are considerably fainter than those in most Sc galaxies of comparable mass.

Are there any nearby galaxies with H II region populations which are similar to the Galactic population? M31 is close. It does not possess any of the bright H II regions that dominate the giant Sc galaxies, but it also contains few if any of the luminous high surface brightness Galactic regions like Carina and NGC 3603 (Pellet *et al.* 1978; Kennicutt, Hodge, and Walterbos, in preparation). The Galaxy's H II region population thus appears to be intermediate between that of M31 and that of a giant Sc, such as M101. Of the galaxies we have surveyed (Hodge and Kennicutt 1983), those whose brightest H II regions seem to be the closest to the Galactic objects are Sbc systems such as NGC 5055 and NGC 7331, or Sb's such as M81. Measurements of the luminosities of the brightest H II regions in galaxies of different types (Kennicutt 1981, 1984) show a strong gradient with Hubble type, with the Galactic regions corresponding most closely to the intermediate (Sbc) types. Unfortunately, even the nearest Sbc galaxies are so distant ($> 10 \text{ Mpc}$) that their H II regions are only marginally resolved, making a direct comparison with the Galaxy difficult. The existing evidence, however, clearly indicates that the contrast between the Galaxy and the other Local Group members is a morphological-type effect, and the Galactic H II region population is probably not unusual for a spiral of its type.

VI. CONCLUSIONS

The main purpose of this paper has been to supply a homogeneous set of data on the properties of giant H II regions in nearby galaxies, with a minimum of interpretation. Nevertheless, several general conclusions can be drawn immediately from these data. While many of them are common knowledge among workers in this field, it is probably useful to summarize some of the basic results concerning the structure of the giant extragalactic H II regions and their relationship to Galactic regions.

The giant extragalactic H II regions are a very heterogeneous group of objects, at least as diverse in their properties as their smaller Galactic counterparts, yet quite distinct from the most familiar Galactic H II regions. The various types of extragalactic regions are distinct from compact Galactic H II regions, and from each other, in terms of at least three, largely independent observables: luminosity, density, and morphology. This conclusion has important implications for understanding the structure and formation of these large star-forming regions. One cannot, as has often been presumed in the past, manufacture the giant H II regions simply by adding O stars to an Orion or Lagoon nebula, or by loosely clumping several dozen of those objects into a large composite region.

The independent variation of luminosity, characteristic density, and radial structure in the H II regions offers some clues as to what physical variables are important in determining their physical properties. From direct implication, two are the density of the parent gas cloud itself and the ultraviolet

luminosity of the embedded star cluster. While the properties of the ionizing stars and the surrounding ionized gas region are partially coupled to one another, we observed order-of-magnitude differences in density at constant luminosity and vice versa, suggesting that other variables are important as well. One major shortcoming of this analysis is that we can study only the ionized component of the interstellar cloud. Other parameters that are crucial in influencing the evolution and structure of Galactic regions, such as the properties of the molecular and neutral gas components, cannot be reliably studied in these objects at the present time. It seems likely, however, that the cold components may play an important, if not dominant, role in accounting for the diversity of nebular properties observed here.

While there is an enormous diversity in the properties of the H II regions in different galaxies, objects within individual galaxies (or regions within large galaxies) tend to be much more homogeneous. This result suggests that the global conditions of the interstellar medium in a galaxy (physical and dynamical) are an important determinant of the structure of the star-forming regions. This is illustrated most directly by the statistics of the ring nebulae, but systematic trends in nebular morphology, ionizing luminosity, and mass are seen throughout the sample. While most theoretical work on star formation has treated the problem as a local process, it should be recognized that many of the gross structural properties of a star-forming region are determined largely by global factors. Admittedly this general result is only weakly supported by the small sample of H II regions presented here. A future paper on H II region populations in nearby spirals will examine the conclusion in more detail.

While it was convenient in this paper to subdivide the extra-

galactic H II regions into several morphological and physical classes, there appears to be a continuous range of H II region properties over this diverse range. In particular, the luminosity function of Galactic H II regions appears to overlap smoothly with the sequence of giant H II regions observed in external galaxies. While the largest and brightest "supergiant" H II regions are impressive objects, especially by Galactic standards, the limited available evidence suggests that they are simply the largest members of their class, not a distinct physical class of H II regions in themselves.

Finally, despite the similarities between many of the giant Galactic and extragalactic H II regions, the results here should lay to rest any suggestion that the apparent differences between the largest Galactic and extragalactic H II regions are entirely observational, rather than physical, in origin. Nothing approaching 30 Doradus, or the large M101 complexes, for example, is present in the Galaxy. This difference is consistent with the morphological-type dependence of H II region properties in external galaxies.

I am indebted to several colleagues for very helpful comments and suggestions during the course of this work, especially You-Hua Chu, John Dickey, Paul Hodge, and Bill Keel. I also wish to thank George Jacoby for generously obtaining a plate of M31 for me during his own observing time. Chris Faust and Rich McLaughlin of the University of Minnesota Space Science Graphic Arts Center performed the heroic task of constructing Figure 1, and their efforts are greatly appreciated. This research was supported by grants AST81-11711 and AST81-11711A01 from the National Science Foundation, and by an award from the Alfred P. Sloan Foundation.

REFERENCES

- Benvenuti, P., Casini, C., and Heidmann, J. 1979, *Nature*, **282**, 272.
 Boulesteix, J., Courtes, G., Laval, A., Monnet, G., and Petit, H. 1974, *Astr. Ap.*, **37**, 33.
 Braunsfurth, E., and Feitzinger, J. V. 1983, *Astr. Ap.*, **127**, 113.
 Brocklehurst, M. 1971, *M.N.R.A.S.*, **153**, 471.
 Castor, J., McCray, R., and Weaver, R. 1975, *Ap. J. (Letters)*, **200**, L107.
 Caulet, A., Deharveng, L., Georgelin, Y. M., and Georgelin, Y. P. 1982, *Astr. Ap.*, **110**, 185.
 Celnick, W. E. 1983, *Astr. Ap. Suppl.*, **53**, 403.
 Chu, Y.-H. 1982, *Ap. J.*, **255**, 79.
 ———. 1983, *Ap. J.*, **269**, 202.
 Davies, R. D., Elliot, K. H., and Meaburn, J. 1976, *Mem. R.A.S.*, **24**, 379.
 Fitzpatrick, E. L., and Savage, B. D. 1983, *Bull. AAS*, **15**, 681.
 Gallagher, J. S., and Hunter, D. A. 1983, *Ap. J.*, **274**, 141.
 Gardner, F. F., Milne, D. K., Mezger, P. G., and Wilson, T. L. 1970, *Astr. Ap.*, **7**, 349.
 Goss, W. M., and Radhakrishnan, V. 1969, *Ap. Letters*, **4**, 199.
 Goss, W. M., and Shaver, P. A. 1970, *Australian J. Phys. Ap. Suppl.*, **14**.
 Gum, C. S., and de Vaucouleurs, G. 1953, *Observatory*, **73**, 152.
 Habing, H. T., and Israel, F. P. 1979, *Ann. Rev. Astr. Ap.*, **17**, 345.
 Hodge, P. W. 1983, *A.J.*, **88**, 1323.
 Hodge, P. W., and Kennicutt, R. C. 1983, *A.J.*, **88**, 296.
 Israel, F. P. 1976, Ph.D. thesis, University of Leiden.
 Israel, F. P., Gatley, I., Mathews, K., and Neugebauer, G. 1982, *Astr. Ap.*, **105**, 229.
 Israel, F. P., and Kennicutt, R. C. 1980, *Ap. Letters*, **21**, 1.
 Keel, W. C. 1982, *Pub. A.S.P.*, **94**, 765.
 Kennicutt, R. C. 1979, *Ap. J.*, **228**, 394.
 ———. 1981, *Ap. J.*, **247**, 9.
 ———. 1983, *Ap. J.*, **272**, 54.
 ———. 1984, in preparation.
 Kennicutt, R. C., Balick, B., and Heckman, T. 1980, *Pub. A.S.P.*, **92**, 134.
 Kennicutt, R. C., and Hodge, P. W. 1980, *Ap. J.*, **241**, 573.
 Kennicutt, R. C., and Kent, S. M. 1983, *A.J.*, **88**, 1094.
 Klein, U., Grave, R., and Wielebinski, R. 1983, *Astr. Ap.*, **117**, 332.
 Koornneef, J. 1978, *Astr. Ap.*, **64**, 179.
 Lasker, B. M. 1977, *Ap. J.*, **212**, 390.
 ———. 1979, *Pub. A.S.P.*, **91**, 153.
 Massey, P., and Hutchings, J. 1983, *Ap. J.*, **275**, 578.
 McCall, M. L. 1982, Ph.D. thesis, University of Texas.
 McKee, C. F., Van Buren, D., and Lazareff, B. 1984, *Ap. J. (Letters)*, **278**, L115.
 Meaburn, J. 1979, *Astr. Ap.*, **75**, 127.
 ———. 1980, *M.N.R.A.S.*, **192**, 365.
 Melnick, J. 1977, *Ap. J.*, **213**, 15.
 Mezger, P. G., and Henderson, A. P. 1967, *Ap. J.*, **147**, 471.
 Mezger, P. G., Schraml, J., and Terzian, Y. 1967, *Ap. J.*, **150**, 807.
 Mills, B. Y., Turtle, A. J., and Watkinson, A. 1978, *M.N.R.A.S.*, **185**, 263.
 O'Connell, R. W., and Mangano, J. J. 1978, *Ap. J.*, **221**, 62.
 O'Dell, C. R., and Castenada, H. O. 1984, preprint.
 Oster, L. 1961, *Ap. J.*, **134**, 1010.
 Osterbrock, D. E., and Flather, E. 1959, *Ap. J.*, **129**, 26.
 Panagia, N. 1973, *A.J.*, **78**, 929.
 Parker, R. A. R., Gull, T. R., and Kirschner, R. P. 1979, *An Emission-Line Survey of the Milky Way* (NASA SP-434).
 Pellet, A., Astier, N., Viale, A., Courtes, G., Maucherat, A., Monnet, G., and Simien, F. 1978, *Astr. Ap. Suppl.*, **31**, 439.
 Sandage, A. R., and Tammann, G. A. 1974, *Ap. J.*, **190**, 525.
 Savage, B. D., Fitzpatrick, E. L., Cassinelli, J. P., and Ebbets, D. C. 1983, *Ap. J.*, **273**, 597.
 Schraml, J., and Mezger, P. G. 1969, *Ap. J.*, **156**, 269.
 Sivan, J. P. 1974, *Astr. Ap. Suppl.*, **16**, 163.
 Skillman, E. 1984, Ph.D. thesis, University of Washington.
 Skillman, E. D., and Balick, B. 1984, *Ap. J.*, **280**, 580.
 van den Bergh, S. 1981, *A.J.*, **86**, 1464.
 Viallefond, F., Allen, R. J., and Goss, W. M. 1981, *Astr. Ap.*, **104**, 127.
 Viallefond, F., Donas, J., and Goss, W. M. 1983, *Astr. Ap.*, **119**, 185.
 Walterbos, R., and Schwing, P. 1984, in preparation.